Cement and Concrete Research 42 (2012) 567–576

Contents lists available at SciVerse ScienceDirect

Cement and Concrete Research

journal homepage: http://ees.elsevier.com/CEMCON/default.asp

Effects of uniaxial stress on alkali–silica reaction induced expansion of concrete

Cyrille F. Dunant [a,*], Karen L. Scrivener [b]

[a] University of Toronto, Galbraith Building, 35 St. George street, Toronto, Canada M5S 1A4
[b] EPFL STI IMX LMC, MXG 232 (Bâtiment MXG), Station 12, CH-1015 Lausanne, Switzerland

ARTICLE INFO

Article history:
Received 9 June 2011
Accepted 15 December 2011

Keywords:
Alkali–aggregate reaction (ASR) (C)
XFEM
Long-term performance (C)
Mechanical properties (C)
Modelling (E)

ABSTRACT

ASR affected concrete in real structures is usually subject to loads which affect the macroscopic expansion of the material. An experimental study was undertaken using sensors embedded in reactive and non-reactive samples loaded on modified creep frames. Numerical analysis was used to link micro-structural damage under the load to expansion. We show that load influences the micro-crack propagation, which changes the shape of the expansion curve.

1. Introduction

The maintenance and scheduling of repairs on structures affected by the alkali–silica reaction (ASR) require accurate and reliable prediction of the concrete expansion due to the reaction. The free expansion of concrete samples can be easily monitored in the laboratory. This can be done using fresh samples made with the same mix design as the one used in the structure, or in the case of mass concrete, cores can be extracted directly and residual expansion measured. However, various external parameters can affect the expansion and damage evolution in the structure itself, notably temperature, relative humidity and the stress state of the concrete. Of these parameters, stress is perhaps the least well understood.

Several experimental studies have been published in which the concrete has been subjected to uniaxial stress. A common feature of those studies is that the expansion is suppressed in the direction of the load for high enough applied stresses. This stress is found to lie, with considerable variation, between 3 and 10 MPa [1-3]. This observation has been the basis of several models, as for example in the works of Léger et al. [4] or of Capra and Bournazel [5] who introduce a correction function which depends on the stress. The cause of this suppression of the expansion is however not well understood, as the stresses which are required to prevent all expansion are higher than the swelling pressure applied by the ASR gel. Binal measured the free pressure exerted by artificial gels and found it to lie in the 0.1 to 2.7 MPa range [6], consistent with earlier measures [7] and more recently by Berra et al. [8], below the pressure required to eliminate the expansion along the direction of the applied stress. Using SEM to study specimens, Larive concluded that the pressure does not inhibit the reaction but only the expansion [9]. Furthermore, the expansion in the directions transverse to the loading is also affected. Berra in particular found that the effect of the applied load on the transverse expansion depends on the aggregate type and can be non-monotonic [8].

To account for the effect of loading on transverse expansion, more elaborate models were proposed. Saouma and Perotti proposed to redistribute the expansion along the principal stress directions based on a set of factors which they obtained by fitting the experiments from Multon [10]. Based on the underlying assumption that anisotropy is due to oriented cracking at the micro-scale, Grimal et al. introduced an anisotropic damage model [11]. Both models are driven by an ageing parameter which prescribes the degradation of mechanical properties and swelling based on external parameters, such as humidity and temperature. However, these approaches are semi-empirical in nature and lack predictive power in the general case. For example, Winnicki shows that the coupled effect of mechanical degradation and restraint is difficult to model using continuum approaches, and fails for high levels of reinforcements [12]. More importantly, they base their constitutive models on the assumption that aggregates react on their surface and fill the surrounding porosity before initiating damage, after which damage parameters along the principal directions are calculated independently.

The expansion must be related to the micro-structural evolution as the morphology of damage at the micro-scale has been shown to depend on the aggregate type [13,14]. Fast reacting aggregates are characterised by the formation of gel on their surface, which causes the paste to crack at the onset of the reaction; slow-reacting aggregate forms gel pockets inside the aggregates, and the aggregates undergo

* Corresponding author. Tel.: +1 416 978 7863; fax: +1 416 978 2077.
E-mail addresses: cyrille.dunant@utoronto.ca (C.F. Dunant), karen.scrivener@epfl.ch (K.L. Scrivener).

0008-8846/$ – see front matter © 2011 Elsevier Ltd. All rights reserved.
doi:10.1016/j.cemconres.2011.12.004

significant cracking before damage reaches the paste. All the models cited above implicitly assume fast reacting aggregates which react on their surface. ASR models of micro-structural degradation have been proposed by the authors [14,15], and can predict the free expansion of laboratory samples, also for slow-reacting aggregates. These models account for the damage morphology and evolution inside the aggregates. This study tries to link external loads to micro-cracking in the aggregates and paste using numerical analysis as well as new data from instrumented samples subject to uni-axial load.

The experimental set-up presented in this paper allowed continuous monitoring of samples from embedded sensors. The samples themselves were kept immersed in simulated pore solutions, which reduces shrinkage, leaching and generally allows measures to be very stable.

2. Materials and methods

Two aggregates were used in this study. The first is a known reactive aggregate which was extensively studied by Ben Haha [16], the other is non-reactive. Both aggregates are mixed-mineralogy Alpine aggregates, but the reactive aggregate consists mostly of chloritic schist [17].

The aggregates were crushed and sieved. The size fractions were then recombined to best approach the Bolomey reference curves [18] (particle size distribution of the fraction and their percentage in the mix are given in Fig. 1).

The w/c was 0.43 and, to improve fluidity, 1% in mass of Rheobuild 5500 was added. The cement used was a CEM I low alkaline cement from Holcim (Pur 4) with 0.5% Na_2O_{eq} wt. of alkalies. All experiments were run with cement from the same batch. This cement was chosen so the alkali content of the initial mix could be controlled with an external addition of sodium hydroxide. The additional sodium hydroxide was added in the mix water to reach a total of 0.9% of the cement mass in alkalies. The mixing protocol is described in Table 1. The samples were cast and then kept for 28 days in a fog room at 20 °C.

After this cure, the samples were placed in creep frames and subjected to 0, 5, 10 and 15 MPa loads. There were 3 concrete cylinders (height 335 mm, diameter 160 mm) in each column: a non-reactive sample on top and two reactive samples at the bottom. The load in each column was kept constant by hydraulic pressure. The non-reactive samples allowed us to distinguish strains due to creep from the expansion induced by ASR. The creep frames were modified by adding stainless steel supports and perspex vessels to maintain the samples in 0.125 mol/l NaOH solutions (Fig. 2). The concentration in Na^+ in cement pore solutions has been measured in the literature between 50 mmol/l and 100 mmol/l, and the concentration of K^+ at around 550 mmol/l [19]. To minimise leaching, whether from the paste to the curing solution or in the other direction, the solutions should have the same composition. However, using too much alkalies can induce non-linear effects on the expansion. As a compromise, the curing solution was a concentration at the low end of what is described in the literature, so that leaching is minimised, but the reaction not otherwise accelerated. The whole set up was placed in a temperature-controlled room at 38 °C.

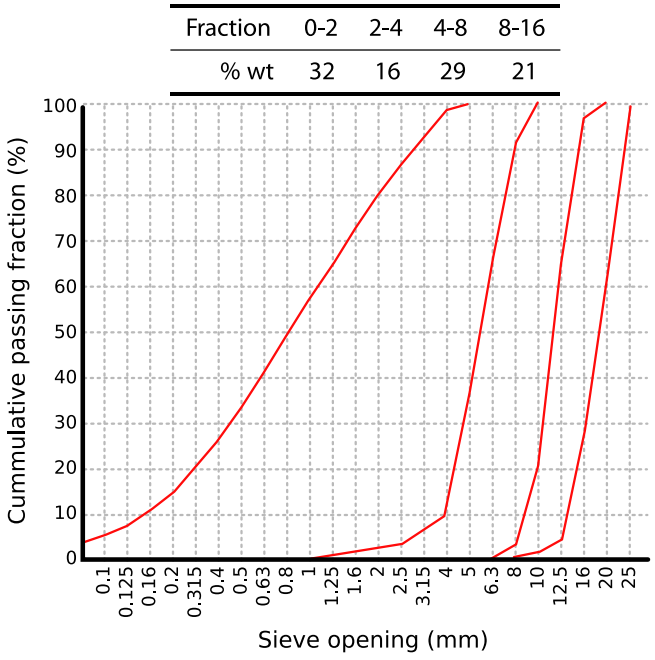

Fig. 1. PSD of the aggregate fractions used as well as the weight fraction of each class.

Table 1
The long initial cure in the protocol is intended to minimise paste hardening during the development of ASR.

Mixing	• Aggregates and cement for 1 min at slow speed • Add water + NaOH for 1 min at slow speed • 2 min at high speed • Half-fill moulds, vibrate • Fill moulds, vibrate • Smooth surface, cover, place in humid conditions
Early cure	De-mould at 24 h, place in fog room until 28 days
Cure	Place in 0.150 mol·l^{-1} alkaline solutions at 38 °C
Measure	Continuous on-line measurements

Due to the immersion of the samples, normal external measures of expansion could not be made and the expansion of the samples was monitored internally with fibre optic sensors. The moulds were pre-instrumented, with the sensors held by steel wires (Fig. 2). Once the moulds were filled, the wires were removed. A preliminary set of samples was prepared using this protocol. These samples were split by a Brazilian test and no defects were observed near dummy sensors. The same procedure was used to inspect the sensors in the experimental samples after the experiments: and again no visible defects were found.

Fig. 2a) and b) shows the set-up and the position of the sensors in the samples. The sensors embedded in each sample placed in the loading frame were:

- A radial strain gauge also containing a temperature sensor. The elongation is measured using a Bragg grated optical fibre (length 67.5 mm). Part of the optical fibre containing the Bragg grating is arranged in a tube. The grated part is in tension between the two ends of the tube and the tube ends are rigidly fixed to a host material. To this sensor is affixed a temperature sensor. The temperature sensor allows the correction of small strain fluctuations due to variations of the ambient temperature.
- A longitudinal strain gauge (optical fibre length 100 mm) which functions in the same way as described above, but without a temperature sensor.
- A computer which logged the sensor values every 20 min.

The resolution of both captors is 0.001 mm. To minimise the effects of friction between the samples, the sensors were placed outside the 45 degree cones defined by the bases of the samples. The strain gauges are longer than the side of a typical representative elementary volume of concrete (4 times the aggregate maximum diameter: REV side 64 mm).

The coefficient of thermal expansion was calibrated from the strains reported at 20 °C and 38 °C before the stresses were applied. The coefficients of thermal expansion found were different whether the samples were prepared with the non-reactive aggregates ($\alpha = 0.011$ mm·m^{-1}·K^{-1}) or with the reactive ones ($\alpha = 0.08$ mm·m^{-1}·K^{-1}). The moduli of the samples were not measured.

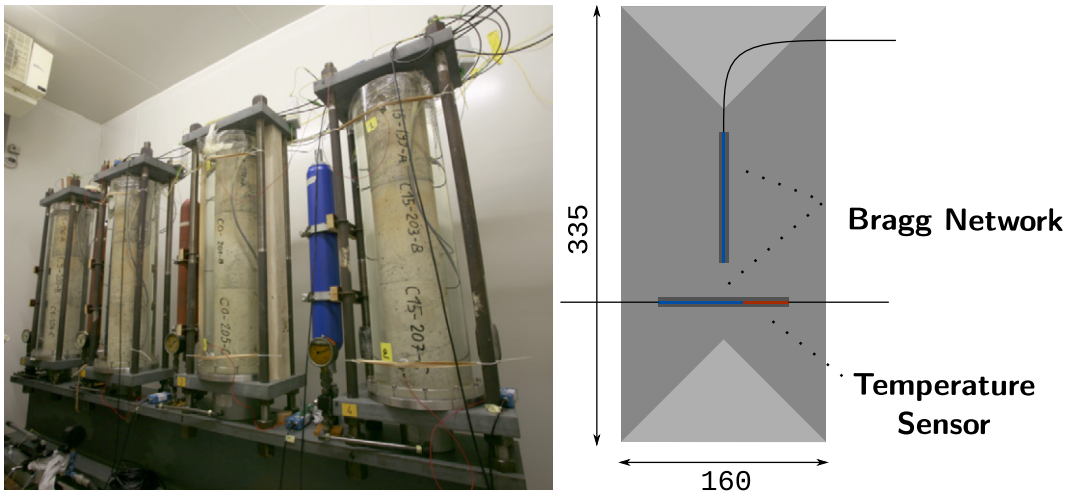

Fig. 2. Samples in the loading frame, schematic of the sample instrumentation. In light grey, the 45 degree cones which mark the location of the disturbed regions.

3. Results

The alkaline environment in which the samples were placed caused the captors of certain of the samples to fail when their seals started to leak. We only present the results from complete time series (Fig. 4). The dispersion, displayed as a light band in the figures, was estimated by comparing the partial time series of the companion reactive samples. The dispersion is much lower than the one reported in the works of Larive [9] due to the immersion of the samples, which eliminates variations due to imperfect relative humidity control. Furthermore, the samples were undisturbed during the duration of the experiment, and strain variations due to temperature fluctuations could be compensated. Finally, the low dispersion can be explained by the scale at which cracking occurred. As the aggregates used are slow reacting aggregates, the cracks caused by the reaction are all micro-cracks in the aggregates and paste. No macroscopic cracks were observed at the surface of the samples during the duration of the experiments.

To compute the width of the error band, the maximum observed difference between matched experimental series was taken as the half of the bandwidth for all samples. As visible in Fig. 3, this value is 0.1 mm/m, which is the maximum of 6 pairs of matched samples, making the bands 0.2 mm/m wide. In this experimental setup a single parameter, the applied load, is varied, therefore smooth trends observed across conditions are likely to be significant.

The longitudinal and lateral expansions measured by the sensors for samples cured under the different loads are shown in Fig. 4. These values have been corrected for thermal expansion. The expansions for the 10 MPa load showed two sudden steps. It was assumed that these corresponded to small amounts of slip of the sensors. These steps were removed from the curves.

Under the loading conditions used the samples exhibit significant creep. The non-reactive samples, cured under the same conditions as the reactive ones, were used to provide a measure of the creep. The viscous deformation of the non-reactive samples (Fig. 5a) was subtracted from the total deformation of the reactive samples, assuming that the ASR did not affect significantly their creep. Since the load was controlled to stay at a constant value, the stress state of the paste would not be affected by ASR on average: more load coming from the reaction would be compensated by less load coming from the pressure cell. Fig. 5 shows the deformation of the samples with and without creep. With the creep removed, no longitudinal expansions remain for loads above 5 MPa other than due to the elastic deformation of the samples. Finally, the initial elastic deformation imposed by the load was subtracted and only the deformation due to ASR is plotted in Fig. 6.

After a year in immersion, the samples reached a plateau in their expansion. The final values measured after the samples had stopped expanding are reported in Table 2 and plotted in Fig. 7. This illustrates the relative effect of ASR versus the combined effects of ASR, elastic deformation and creep.

For the unloaded samples, the lateral and longitudinal expansions differ somewhat, probably due to some anisotropy introduced in the casting process. This effect has previously been reported [20]. When the samples are under load, the longitudinal expansion is reduced as expected, but so is the lateral expansion. When the load is increased further, the longitudinal expansion goes to 0, but the lateral expansion increases. This behaviour is at odds with the idea of a "redistribution" of the expansion, as described by Larive [9]. As described by Berra, this may be due to the aggregate type [8].

From a load between 5 and 10 MPa the expansion in the direction of the load is completely inhibited. The magnitude of the lateral expansion increased from 5 to 15 MPa and the initiation of lateral expansion occurred earlier for higher loads. The elastic deformation accounts for a small part of the lateral expansion so ASR is the most significant there (Fig. 8).

The experimental results indicate that there is a difference of nature in the expansions under free and loaded conditions. For loads between 5 and 15 MPa, increasing the load changes the kinetics of expansion. A simple analysis was done where the linear part of the expansion was fitted with a line and the inflexion point marked. This shows clearly the acceleration of the expansion under increased loads beyond 5 MPa (Fig. 9).

As the sensors gave the strain in two directions, the relative volume (R_V) of the cylinders could be computed as:

$$R_V = \frac{(l_0 + \Delta l) \times (r_0 + \Delta r)^2}{l_0 \times r_0^2} \quad (1)$$

with l, l_0 the longitudinal sensor length, respectively initial length, r, r_0 the lateral sensor length, respectively initial length. The results are plotted in Fig. 10. This gives the ratio of the volume after the reaction has occurred over the initial volume. It assumes that the expansions in all the lateral directions are the same.

The volumetric variations under 10 MPa and 15 MPa loads are only due to lateral expansion as no longitudinal expansion is observed. The expansions measured are well beyond the strain limit of the material. It can therefore be assumed that the expansion observed comes from the opening of cracks, micro or macro. To assess this effect, a numerical model was used.

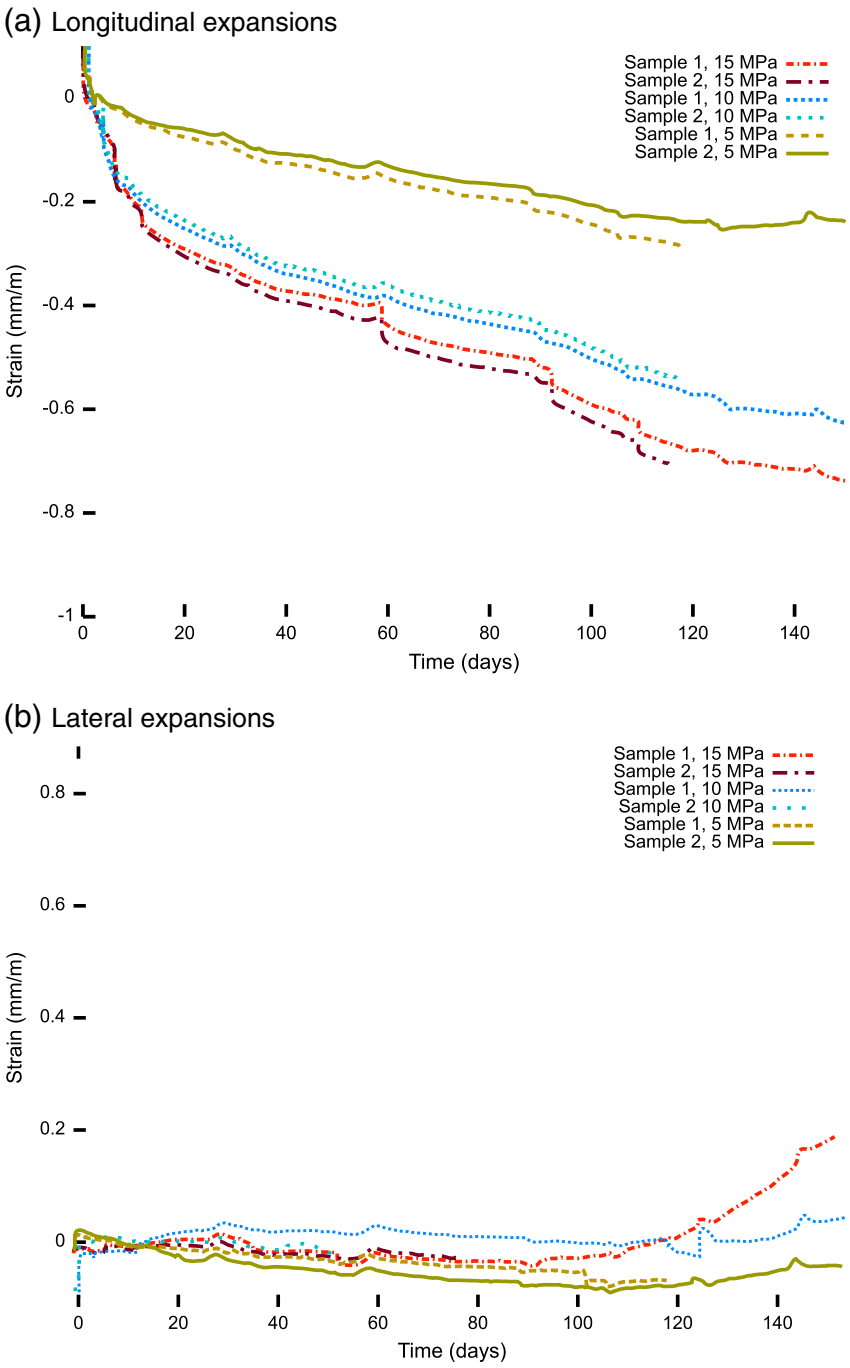

Fig. 3. Time series for expansions for all loaded experimental samples. These series have not been corrected for temperature effect.

4. Numerical model and discussion

The numerical model used is based on the AMIE extended element framework [21]. This model is constructed around an explicit, if idealised, representation of a concrete slice. First, a set of aggregates with the correct size distribution is generated. Then the aggregates are placed in the virtual sample slice using a random placement algorithm. The geometry is meshed and mechanical behaviours are attributed to each element. The behaviours are slightly randomised in each element to reproduce the inhomogeneities of the cement paste and aggregates. Gel pockets are distributed randomly in each aggregate. The gel pocket density is approximately constant and based on microscopic observations.

The gel pockets are ideally-bonded elastic inclusions with an imposed isotropic strain [14]. As their size makes meshing impractical, extended finite elements [22,23] are used to model the interface between the gel and the surrounding material. This method allows a good precision despite the relatively few elements used to model each gel pocket.

The microscopic material damage is simulated using a non-local damage method [24], and the resulting macroscopic expansion calculated. This approach models ASR explicitly, and captures well the mechanisms of degradation at the scales considered. A single parameter is fitted: the stiffness of the ASR gel, for which there is no good value published in literature. Based on previous studies [14], a value of 0.7 times that of C–S–H was used. This parameter was fitted for expansion–reaction curves, which did not depend on the kinetics of

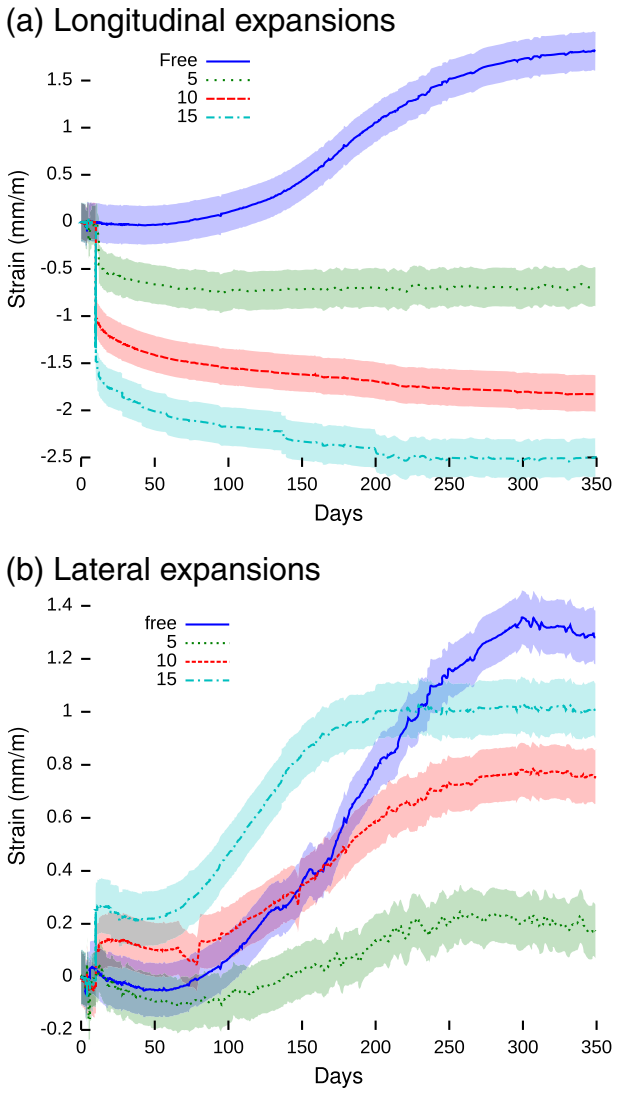

Fig. 4. Compared expansions of samples cured under various uni-axial loads. The lateral expansions increase with the load but remain lower than these observed under unloaded conditions. No visible expansions are observed in the direction of the load.

the expansion. The imposed strain assumes that the gel has double the volume of the original aggregate material. This latter value is well supported by literature [25-27]. The gel stiffness stays constant through the simulation.

The simulations are run assuming plane strain. The mechanical properties for the materials are reported in Table 3. The constitutive relationships for the aggregates and gel are elastic until the equivalent stress reaches σ_{yield}. Then the Young modulus is reduced using a scalar isotropic damage parameter d such that:

$$\begin{cases} \sigma = \mathbf{E}\epsilon = \mathbf{E}_0(1-d)\epsilon \\ \text{such that} \begin{cases} \sigma_{eq} = max\ \bar{\sigma}_i = \sigma_{yield} & if\ d<d_{crit} \\ E = 0 & if\ d \geq d_{crit} \end{cases} \end{cases} . \quad (2)$$

The non-local $\bar{\sigma}_i$ are the principal stresses calculated from the smoothed stress fields (ρ the characteristic radius) obtained by:

$$\bar{\boldsymbol{\sigma}} = \frac{\int_0^{2\pi}\int_0^{3\rho} \boldsymbol{\sigma}(r,\theta) e^{-\frac{r^2}{2\rho}} dr d\theta}{\int_0^{2\pi}\int_0^{3\rho} e^{-\frac{r^2}{2\rho}} dr d\theta} \quad (3)$$

The strain of the gel pockets is imposed as stresses:

$$\sigma_{imposed} = \mathbf{E}_{gel}\epsilon_{imposed} \quad where\ \epsilon_{imposed} = \begin{pmatrix} 0.5 & 0 \\ 0 & 0.5 \end{pmatrix}$$

The tension and compression yield stresses are different, and the sign of the principal stresses is considered to select which criterion to apply. The details of the algorithm used to compute damage can be found in [24].

To simulate the progress of the reaction, the gel pockets change their diameter at each step of the simulation. The amount of material reacted is then assumed to vary linearly with time. Experimental correlations obtained in [15,14] corroborate this hypothesis. As in [15], the kinetics of expansion is obtained by assuming 1% of the aggregate is transformed into gel in 210 days.

In a first set of calculations, instead of using a complete microstructure, a single finely meshed aggregate was simulated under free and loaded conditions. These simulations illustrate the effect of the load on crack propagation in the matrix and the aggregates, as well as the interactions between the gel pockets within aggregates.

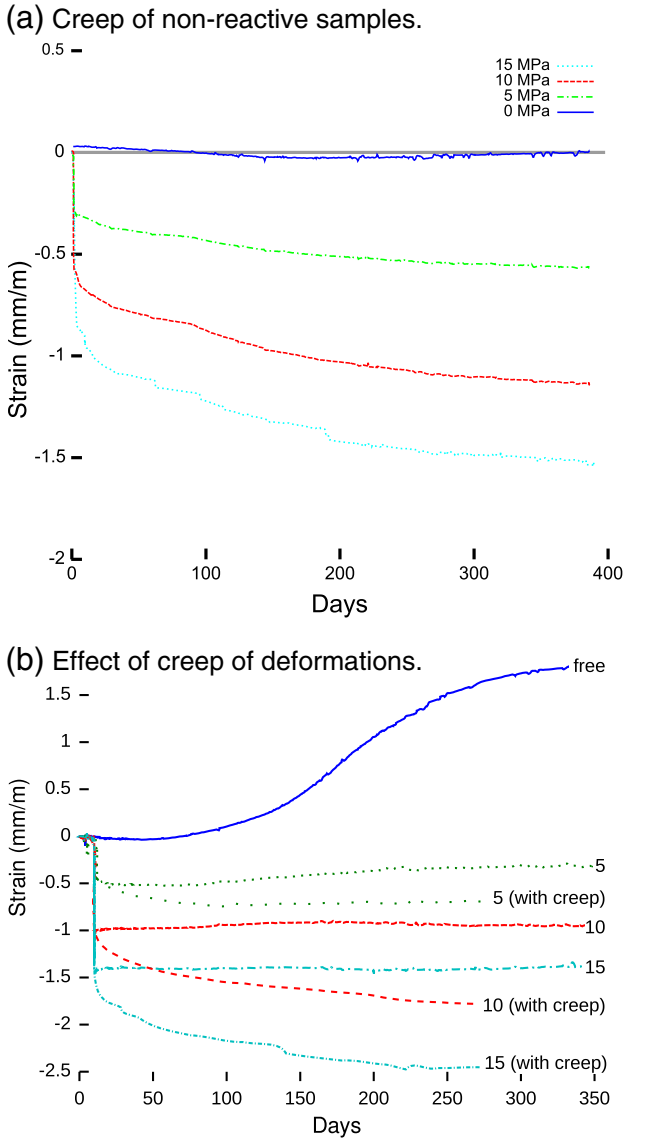

Fig. 5. Effect of the creep on the expansions. The creep was removed using a measure from non-reactive samples cast with the same cement.

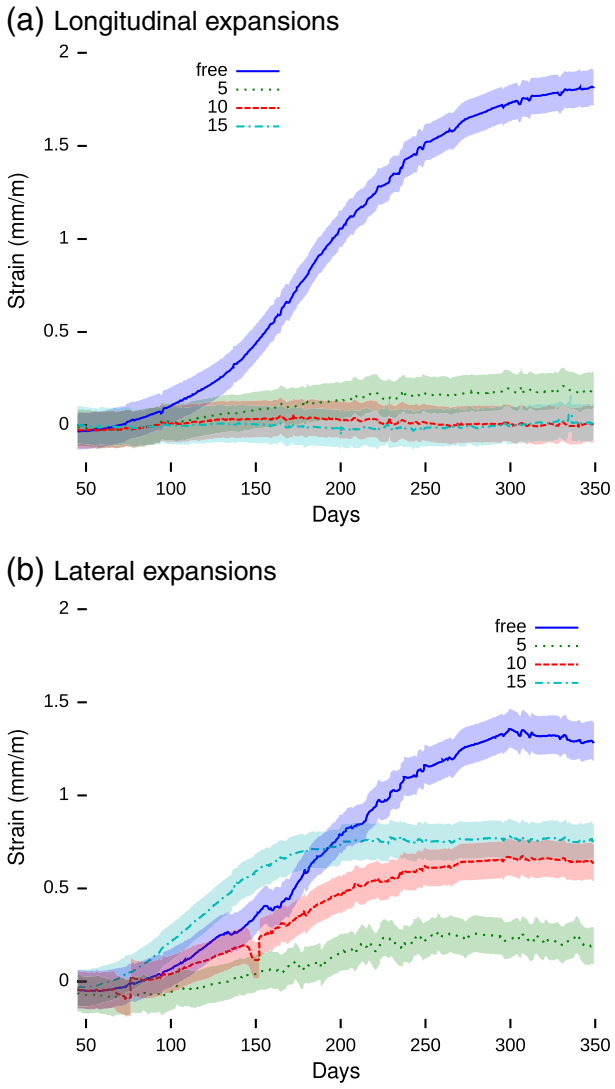

Fig. 6. Lateral and longitudinal expansions of samples due to ASR. Both creep and elastic deformations have been removed. Only the sample under 5 MPa load exhibits any significant longitudinal expansion.

In the unloaded condition, no particular direction of propagation is favoured by the cracks, except for the normal tendency to propagate in directions normal to interfaces. Under the 5 MPa load, the cracking is more pronounced and the cracks initiate more frequently in the aggregate. Notable features of the crack patterns are:

- damage concentration immediately around gel pockets,
- a network of cracks connecting the gel pockets,
- a dense pattern of short radial cracks immediately around the aggregates,
- relatively few main cracks which will grow to the edge of the samples.

Table 2
Final expansions recorded as a function of the load.

Load MPa	Lat. all mm/m	ASR Lat. mm/m	Long. all mm/m	ASR Long. mm/m
0	1.4	1.4	1.6	1.6
5	0.2	0.25	−0.4	0.1
10	0.55	0.7	−1	0
15	0.7	0.9	−1.4	0

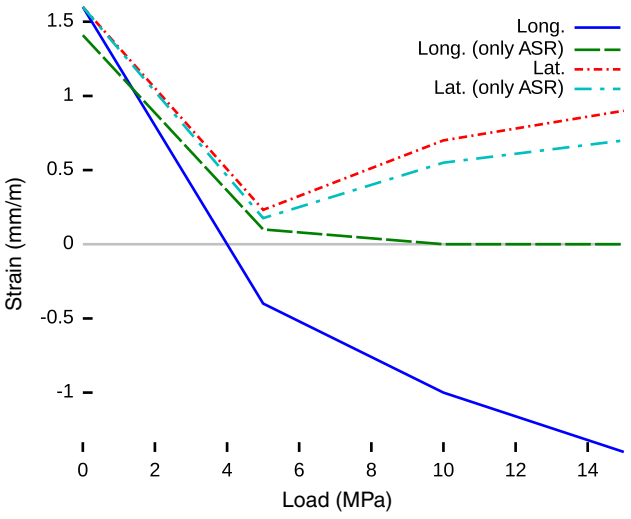

Fig. 7. Final expansions recorded as a function of the load.

Under load, a clear direction of propagation is favoured: parallel to the load. This corresponds to the experimental observations of Larive for macro-cracks on the surface of her samples. In the simulations of single aggregates, the expansion in the direction normal to the axis of loading *increases* compared to the expansion in the unloaded case.

The stress around the gel pockets, calculated by elastic numerical simulation, is in the order of 1 GPa, and the imposed stress on the samples is therefore negligible with respect to the criterion for crack initiation near the gel pockets. This very high stress is due to the small size of the gel pockets and the quasi-incompressible behaviour. When damage is taken into account, this stress never goes above the tensile limit of the aggregate, at which point it is relieved by fracture. However, the stress and strain fields are oriented by the load, and unlike initiation, the crack propagation direction is affected. The most important consequence is that aggregates are more prone to splitting along the load axis (Fig. 11), which explains the faster lateral expansion measured at larger loads.

The second set of simulations, with full PSD, considered loads around the 5 MPa value. These simulations use a fine mesh, with 300,000 degrees of freedom. 5 MPa was considered an important value because our experiments showed that under this load, the longitudinal expansion due to ASR is not completely suppressed, indicating that the transition between damage regimes is not complete.

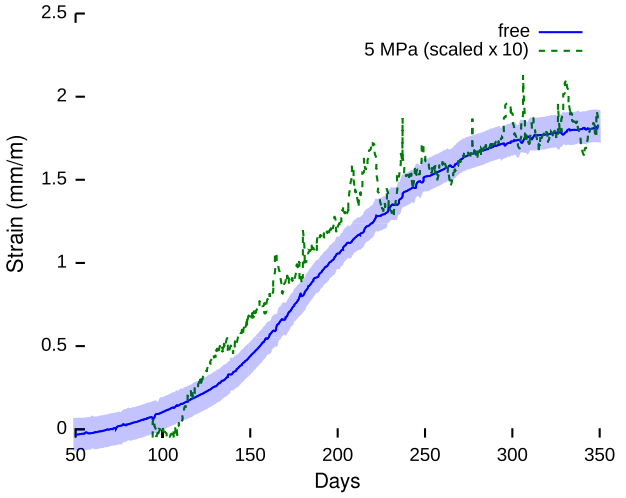

Fig. 8. Comparison of the free lateral expansion and of the lateral expansion under a 5 MPa load. The 5 MPa expansion has been scaled to highlight the similarity in the curve shape.

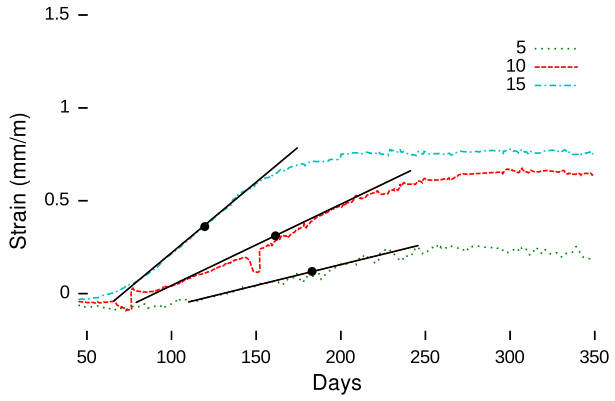

Fig. 9. Linear part of the lateral expansion of loaded samples. The position of the inflexion point is marked with a black dot. The expansion is accelerated by the load.

Control simulation without load had perfectly captured the expansion curve [15,14]. Simulations of expansions under loads of 2.5 MPa, 5 MPa and 7.5 MPa were run. The simulations do not take into account the creep in the paste and are compared with the experimental expansions with the creep removed.

The simulated expansions at a load of 2.5 MPa (Fig. 12) are well in the trend of the observed effect of stress for loads under 5 MPa. This indicates that for such low loads, although the direction of cracking is affected, as demonstrated by lower longitudinal and lateral expansions than the average between the experimental 5 MPa and free expansion curves, the mode of damage remains the same: the shape of the expansion curve is not affected. When the final expansion reported by this simulation is plotted along with the experimental values, it falls very clearly in the trend (Fig. 12c). The simulation also predicts the lower lateral expansion.

The crack patterns for the loads above 2.5 MPa were significantly denser than those observed for simulations of free expansions (Fig. 13). The cracks are also oriented in the direction of the load, as expected. The lower lateral expansions can be explained by the fact that aligned cracks provide space for local lateral deformations which are not translated to global lateral deformation.

At higher loads, the damage-enhancing effect is more pronounced as visible in Fig. 14 and leads to failure of the simulated samples. The simulated samples undergo catastrophic failure after 125 simulated days for a 5 MPa load and after 90 simulated days for the 7.5 MPa load. Fig. 14 illustrates the state of the samples when they fail. The

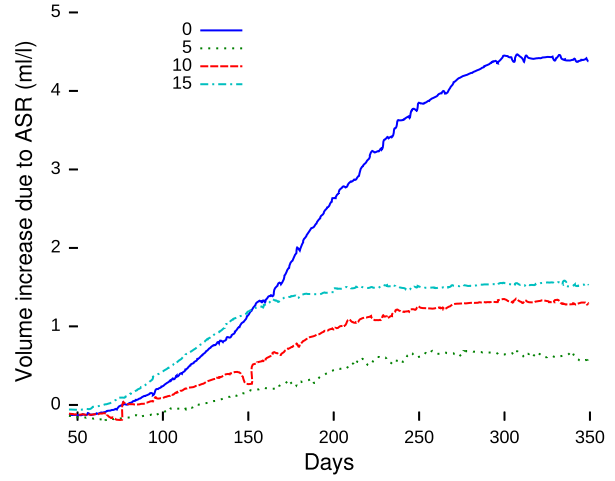

Fig. 10. Relative volume evolution of the reactive samples under different loads. Two regimes are apparent, one between 0 and 5 MPa, which does not inhibit the expansion, and one between 10 and 15 MPa, which does.

Table 3
Mechanical properties of the different materials in the simulation.

	E_0 GPa	ν –	$\sigma_{yield,\ c}$ MPa	$\sigma_{yield,\ t}$ MPa	d_{crit} –	ρ mm
Paste	12	0.3	−23.2	2.9	0.95	0.5
Agg.	59	0.3	−45.6	5.7	0.95	0.5
Gel	21.7	0.5	–	–	–	–

simulations diverge at the same time as the experiments undergo an acceleration of their lateral expansions. At the time of failure, the simulated samples split and as a slip condition had been set on the boundary, they undergo solid body motion and simulations diverged. With dense crack patterns, failure occurs more easily in 2D than in 3D. Further, the damage model used does not account for cracks closing in compression, and this may explain the failure of the model to capture the behaviour at later stages of the reaction.

Further experiments were performed with a gel stiffness value of 0.6 and 0.5 times that of C–S–H to verify whether the cracking was induced by excessively high stresses induced by the gel pockets, but this did not affect significantly the results. Indeed, modelling the free expansion of mortars [14] had shown that the final expansion is not very sensitive to the stiffness of simulated gel, and this was confirmed. Even with the softer gel, the samples underwent failure early in the simulation (Fig. 12d).

At larger loads, experimentally, the samples do not exhibit any longitudinal expansion at all. This means that all the expansion due to the gel in that direction is contained. This in turn indicates that the cracks must almost all be in planes parallel to the direction of the loading. In two dimensional simulations, this will always lead to the sample splitting, as soon as a single line of damaged elements joins the two sides of the sample, which will occur early in the simulation. To prevent this, displacements normal to the axis of loading could be blocked on the loaded boundaries of the sample. However, doing that would not reproduce the experimental boundary conditions.

Despite the limits of the 2D simulations, the following mechanism for the shape of the lateral expansion can be postulated: the orientation of cracks on parallel planes facilitates their merging, and thus the formation and propagation of macro-cracks. This causes the acceleration of the expansion in the lateral direction of the experimental samples. However, cracks tend not to propagate towards compression zones. Thus, although the cracks form and coalesce faster, they must propagate less, which reduces the expansion measured. No experimental sample failed, however, which indicates that the damage is probably overestimated by the simulation.

The low expansions observed experimentally at 5 MPa is probably due to the very specific combination of mechanical properties of the materials, the aggregate type and the morphology of the cracks formed. As the strength of the material was not measured, this result does not indicate that the concrete is less damaged at this load. On the contrary, both the simulations and experiments indicate that load accelerates the damage evolution of the material. In general, although a minimum in the lateral expansion as a function of load can be found for slowly reacting aggregates, as also observed in [8], this minimum should not be expected to be as low as the one reported here.

The morphology of the observed crack patterns could explain the results. Cracks forming around an expanding inclusion form a dense radial pattern over a short distance, as well as causing the opening of a few main cracks. The dense radial pattern is required for strain compatibility. However, this has the effect of enclosing the expanding inclusion in a soft transition zone, which reduces the pressure it exerts on its surroundings, and thus the length of the larger cracks. The interaction between the expanding gel pockets early in the reaction, and the expanding aggregates later on, may cause the transition zone around the gel pockets and aggregates to be larger, and the main

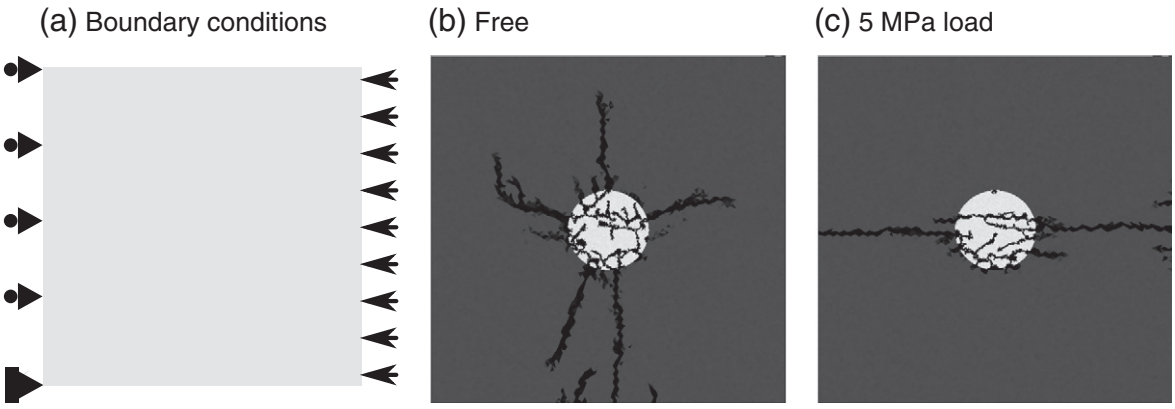

Fig. 11. Crack pattern of a numerical sample with a single inclusion in unloaded and loaded conditions. The cracks are mainly in the paste (dark grey), which is in tension as there are no other expanding aggregates to keep it in compression. **The aggregate** (light grey) is partly cracked, around the gel pockets, but also from cracks which propagated from the paste.

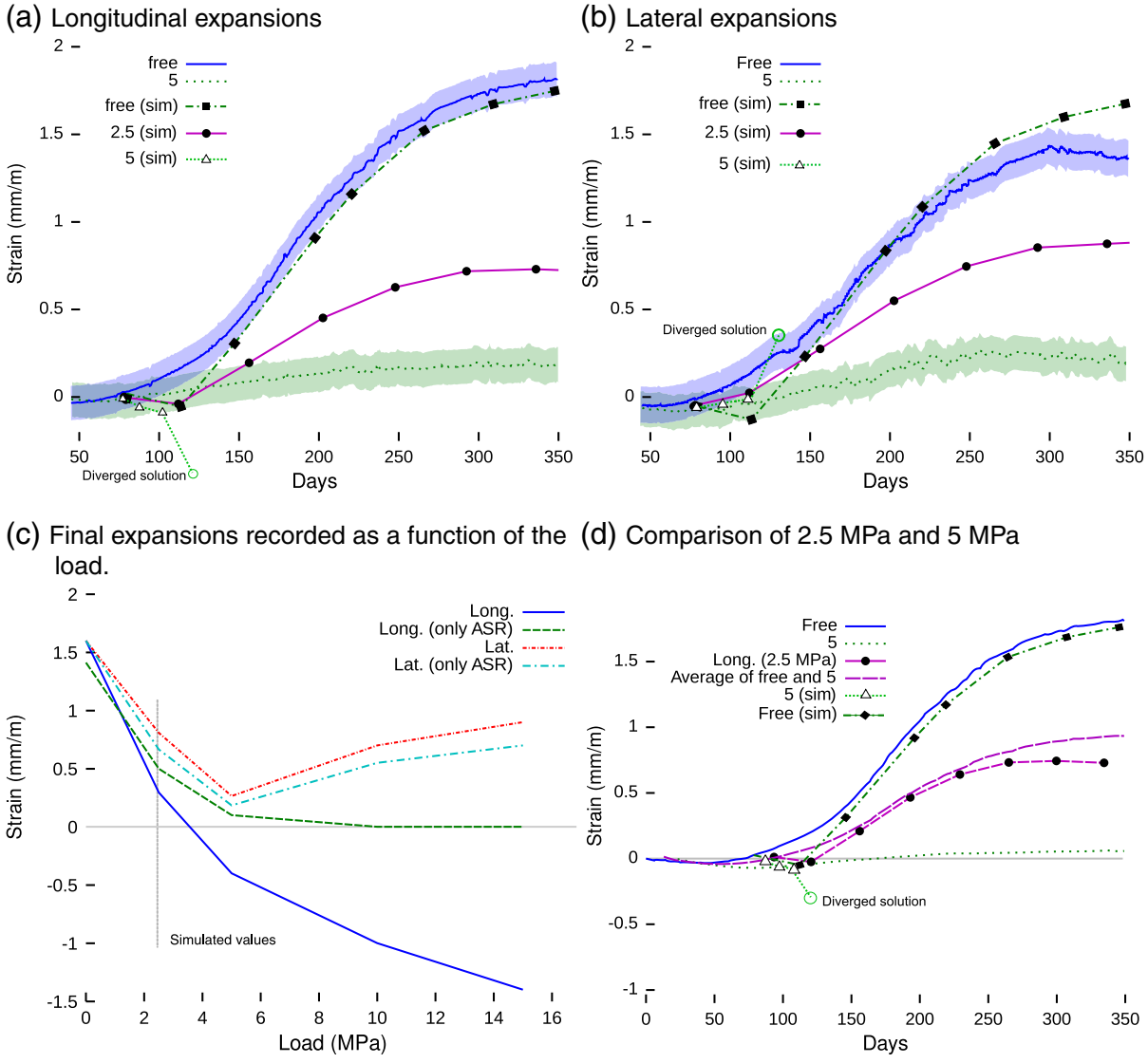

Fig. 12. Simulated expansion under a 2.5 MPa load. As expected, the lateral expansion (a) is slightly lower than the average between the 5 MPa and the free case, as for the lateral (b). (c) Final expansions recorded as a function of the load. The point at 2.5 MPa is simulated and fits perfectly in the different trends, thus validating the model for loads under 5 MPa. (d) Comparison of the expansion under 2.5 MPa and 5 MPa loads and with experiments.

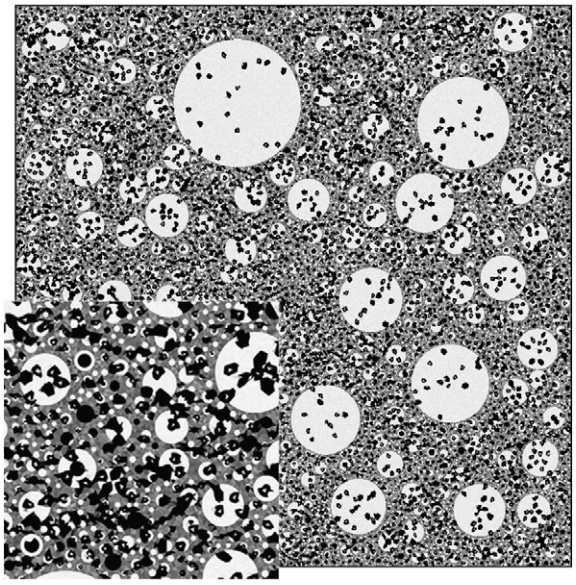

Fig. 13. State of the sample under 2.5 MPa load at the end of the simulation. The cracks are, as in the single inclusion simulations, on average oriented in the direction of the load (→←).

cracks to be smaller. This could result in lower expansion in the direction normal to the loading, compared to free expansion.

5. Conclusion and future work

The effects of uni-axial stress on the expansion of ASR reactive concrete were linked to the orientation and development of micro-cracks in the aggregates and paste. This new understanding of the expansion and degradation mechanism can help develop material-scale models for use in finite element codes and help predict the service life of structures. It is notably found that:

- The expansion is not redistributed, but the applied load forces the orientation of the micro-cracks at the micro-structural level.
- It is found that similarly to what was assumed by Grimal et al. [11], it is not possible to consider damage along the principal axes independently when considering concrete as a homogeneous material, and the expansions along each axes must be computed together.
- Applied stress affects the kinetics of expansion, probably due to accelerated damage evolution under load. It was found that splitting of the aggregates occurred earlier in the simulations when load was applied.
- The lower expansion observed in the lateral direction when longitudinal load is applied is qualitatively and quantitatively reproduced for low stresses by the numerical model. However, no simple explanation for this is proposed by the authors: the phenomenon is probably due to subtle changes in the local damage patterns due to the presence of a large number of aggregates expanding concurrently.

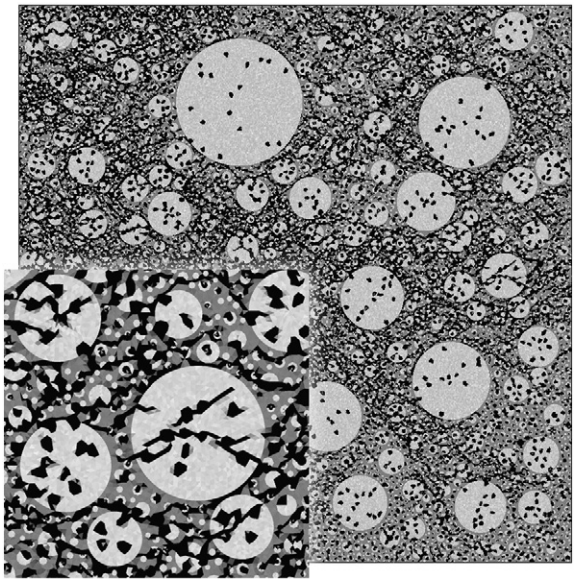

Fig. 14. State of the sample under 5 MPa load at failure. The sample has split and the simulation diverged. Direction of load: →←.

Other observations in the literature exhibit complex relationships between stress and normal expansion, however the low expansions observed under 5 MPa are probably specific to this experimental programme. The relation between the expansion in the lateral direction and the load in the longitudinal expansion is probably due to interactions between aggregates: the local crack patterns, notably, can be significantly different whether aggregates are embedded in paste, mortar, or expanding concrete.

Ongoing development of the damage model could allow simulations of concretes under higher loads. The introduction of a viscous paste behaviour might also help understand the interaction between the cracking and creeping relaxation behaviours.

Acknowledgements

The authors wish to thank the Swiss Federal Office for Energy (OFEN) and the Swiss National Science Foundation (FNS fellowship PBELP2-130912) for their support, financial and otherwise.

References

[1] M.F. Herrador, F. Martínez-Abella, J.R.R. Dopico, Experimental evaluation of expansive behavior of an old-aged ASR-affected dam concrete: methodology and application, Mater. Struct. 41 (2008) 173–188.
[2] I. Mohamed, L. Curtil, S. Ronel-Ldrissi, P. Hamelin, Influence of composite materials confinement on alkali–aggregate expansion, Mater. Struct. 36 (2005) 387–394.
[3] S. Multon, F. Toutlemonde, Effect of applied stresses on alkali–silica reaction-induced expansions, Cem. Concr. Res. 36 (5) (2006) 912–920.
[4] P. Léger, P. Côté, R. Tinawi, Finite element analysis of concrete swelling due to alkali–aggregate reactions in dams, Comput. Struct. 60 (4) (1996) 601–611.
[5] B. Capra, J.P. Bournazel, Modeling of induced mechanical effects of alkali–aggregate reactions, Cem. Concr. Res. 28 (2) (1998) 251–260.
[6] A. Binal, The determination of gel swelling pressure of reactive aggregates by ASPGM device and a new reactive-innocuous aggregate decision chart, Constr. Build. Mater. 22 (1) (2008) 1–13.
[7] C.F. Ferraris, E.J. Garboczi, F.L. Davis, J.R. Clifton, Effect of stress relaxation, self-desiccation, and water absorption on the alkali–silica reaction in low water/cement ratio mortars, the, Cem. Concr. Res. 27 (10) (1997) 1553–1560.
[8] M. Berra, G. Faggiani, T. Mangialardi, A. Paolini, Influence of stress restraint on the expansive behaviour of concrete affected by alklali–silica reaction, Cem. Conc. Res. 40 (2010) 1403–1409.
[9] C. Larive, Apports combinés de l'expérimentation et de la modélisation à la compréhension de l'alcali-réaction et de ses effets mécaniques, Ph.D. thesis, Études Et Recherches Des Laboratoires Des Ponts Et Chaussées (1998).
[10] V. Saouma, L. Perotti, Constitutive model for alkali–aggregate reactions, ACI Mater. J. 103 (3) (2006) 194–202.
[11] E. Grimal, A. Sellier, Y. Le Pape, E. Bourdarot, Creep, shrinkage, and anisotropic damage in alkali–aggregate reaction swelling mechanism—part I: a constitutive model, ACI Mater, J. 105 (3) (2008).
[12] A. Winnicki, S. Pietruszczak, On mechanical degradation of reinforced concrete affected by alkali–silica reaction, J. Eng. Mech. 134 (2008) 611.
[13] J.M. Ponce, O.R. Batic, Different manifestations of the alkali–silica reaction in concrete according to the reaction kinetics of the reactive aggregate, Cem. Concr. Res. 36 (6) (2006) 1148–1156.
[14] C.F. Dunant, K.L. Scrivener, Micro-mechanical modelling of alkali–silica-reaction-induced degradation using the amie framework, Cem. Concr. Res. (4) (2010) 517–525.
[15] C. F. Dunant, Experimental and modelling study of the alkali–silica-reaction in concrete, Ph.D. thesis, École Polytechnique Fédérale de Lausanne (2009).

[16] M. Ben Haha, E. Gallucci, A. Guidoum, K.L. Scrivener, Relation of expansion due to alkali silica reaction to the degree of reaction measured by sem image analysis, Cem. Concr. Res. 37 (8) (2007) 1206–1214.
[17] M. Ben Haha, Mechanical effects of alkali silica reaction in concrete studied by SEM-image analysis, Ph.D. thesis, École Polytechnique Fédérale de Lausanne (May 2006).
[18] J. Bolomey, Granulation et prévision de la résistance probable des bétons, Travaux 30 (19) (1935) 228–232.
[19] B. Lothenbach, F. Winnefeld, Thermodynamic modelling of the hydration of Portland cement, Cem. Conc. Res. 36 (2005) 209–226.
[20] N. Smaoui, M.-A. Bérubé, B. Fournier, B. Bissonnette, Influence of specimen geometry, orientation of casting plane, and mode of concrete consolidation on expansion due to ASR, Cem. Concr. Aggregates 26 (2) (2004) 1–13.
[21] C. Dunant, P.N. Vinh, M. Belgasmia, S. Bordas, A. Guidoum, Architecture trade-offs of integrating a mesh generator to partition of unity enriched object-oriented finite element software, Rev. Eur. Méc. Numér. 16 (2007) 237–258.
[22] N. Moës, J.E. Dolbow, T. Belytschko, A finite element method for crack growth without remeshing, Int. J. Numer. Methods Eng. 46 (1) (1999) 131–150.
[23] I. Babuška, I. Melenk, Partition of unity method, Int. J. Numer. Methods Eng. 40 (4) (1997) 727–758.
[24] C.F. Dunant, P. Kerfriden, S. Bordas, K.L. Scrivener, T. Rabczuck, An algorithm to compute damage from load in composites, Front. Arch. Civil Eng. China 5 (2) (2011) 180–193.
[25] A. Perruchot, P. Massard, J. Lombardi, Composition et volume molaire apparent des gels Ca–Si, une approche expérimentale, C. R. Geosci. 335 (2003) 951–958.
[26] M. Kawamura, K. Iwahori, ASR gel composition and expansive pressure in mortars under restraint, Cem. Concr. Compos. 26 (1) (2004) 47–56.
[27] C.E. Tambelli, J.F. Schneider, N.P. Hasparyk, P.J.M. Monteiro, Study of the structure of alkali–silica reaction gel by high-resolution NMR spectroscopy, J. Non-Cryst. Solids 352 (32) (2006) 3429–3436.